Angewandte Chemie
Eine Zeitschrift der Gesellschaft Deutscher Chemiker

Supporting Information

Identification of Unusual Plumbonacrite in Rembrandt's Impasto by Using Multimodal Synchrotron X-ray Diffraction Spectroscopy

Victor Gonzalez, Marine Cotte, Gilles Wallez, Annelies van Loon, Wout de Nolf, Myriam Eveno, Katrien Keune, Petria Noble, and Joris Dik*

anie_201813105_sm_miscellaneous_information.pdf

Supporting information

1) Experimental methods

Experimental methods were similar to those detailed in [1,2]. In a few words, HR-XRD patterns were acquired at ID22 (ESRF) at 35 keV on paint fragments placed in capillary, and rotated in front of a 1x1 mm² beam. 20 min scans were repeated up to a total acquisition time of 1-4 h to record XRD patterns with a good signal to noise ratio. The exploitable angular range was $2 \leq 2\theta\ (°) \leq 22$ ($0.93 \leq d\ (Å) \leq 10.14$), allowing the measurement of 152 reflections for C and 49 for HC. The main advantages of this configuration are the excellent angular resolution (0.002°) and the absence of preferential orientation, permitting the collection of high quality datasets. XRD patterns were then analysed using the Fullprof suite to derive a precise composition (error bars of about ±1 w% estimated from a C/HC calibration mixture) as well as modelling of the pigment crystallites.

µXRD maps were acquired at the ID13 "microbranch" beamline (ESRF). Samples were either thin (10 µm) sections (cf. Fig. S1) or thick sections, of paint fragments embedded in resin. Samples were mounted vertically, perpendicular to the X-ray beam. The energy of the incident beam was 13.0 keV. The beam was focused to 1.5 µm ver.× 2.2 µm hor. (flux = 8.1011 ph/s) using compound refractive lenses (CRL) mounted in a transfocator. XRD maps were obtained by raster scanning the samples and collecting XRD 2D patterns, in transmission, with a Dectris Eiger 4M single photon counting detector that provides frames with 2070 × 2167 pixels (75 × 75 µm² pixel size) at a rate up to 750 Hz. 2D XRD patterns were azimuthally integrated using the PyFAI software package [3] and XRD maps were analysed with the XRDUA [4] and the PyMca ROI imaging software [5] packages.

2) Preparation of thin section from resin blocks

The preparation of thin sections for µ-XRD measurements was described in detail in [2].

The result of the micro-slicing for the *Bathsheba* sample is presented in Fig. S.1.

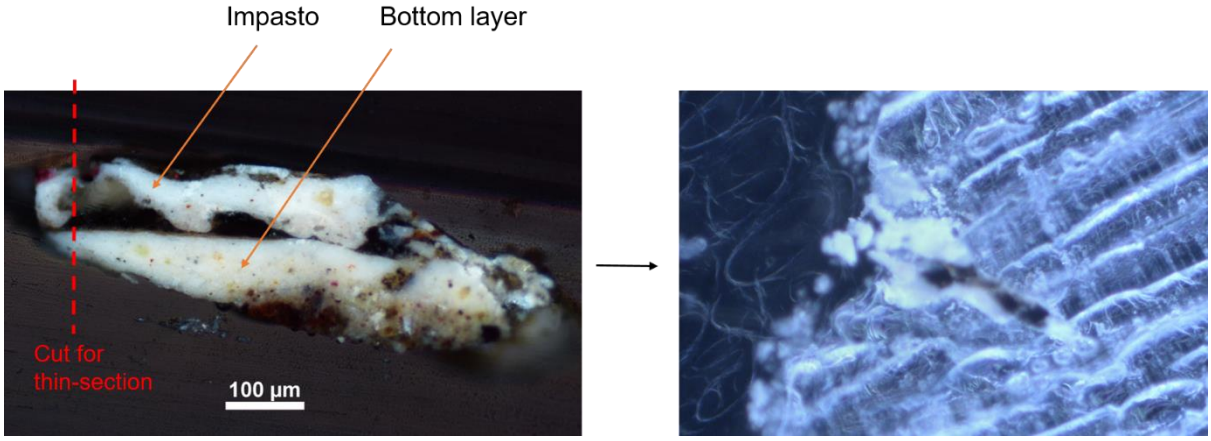

Figure S.1 : Preparation of thin-sections for µ-XRD experiments at ID13.

3) High-angle resolution XRD – Rietveld refinement

For this experiment, the collected data were combined into 0.002° bins for further treatments. The diffraction patterns were analysed by Rietveld refinement using the Fullprof suite [6] on the basis of the crystallographic data (lattice and structural parameters) found in the literature for C [7], HC [8] and PN [9]. While cell parameters were treated as variables to correct the inevitable discrepancies with the previous works, atomic positions and thermal parameters were kept fixed because of the limited number or reflections measured. The Thompson–Cox–Hastings function with spherical harmonics expansion was implemented to fit the anisotropic peaks broadening of the major phases and explore their

microstructure. The reliability factors reached for the main phases were satisfactory, and the main residuals on the difference line mainly resulted from the noise. In particular, the particles' texturing tendency appeared to have been efficiently thwarted by the experimental setting. Quantitative phases analyses were derived from the scale factors to assess the pigments composition. Concerning the pigments microstructure, an estimation of the crystallites' dimensions was attempted on the basis of the peaks broadening, computed referring to the instrumental function plotted from the diffraction pattern of a LaB_6 sample. Anisotropic broadening was ascribed to the sole Scherrer's size effect.

4) Selection of ROIs for crystalline phase mapping

As indicated in the manuscript, for visualization of the crystalline phases distribution within micrometric paint layers, the PyMca ROI imaging software package was used. Background correction was also applied. Regions of interest (ROIs) were selected around a single, but strong and non-overlapped peak for each phase: C(021) : [15.6 ; 15.8 (2θ)], HC(015) : [16.6 ; 16.8 (2θ)] and PN(112) : [16.2 ; 16.4 (2θ)].

5) Reconstruction of [pigment + PbO-siccatived binders]

Fig. S.2 reports the distribution of PN in a thin section of a model painting, prepared following the De Mayerne recipe for “huile de litharge” [10]. This sample was reanalysed by µXRD after nine years of natural ageing [11]. This map shows that PN is mainly concentrated in a large white protrusion, but is also spread all over the paint layer, in aggregates of up to 10 µm.

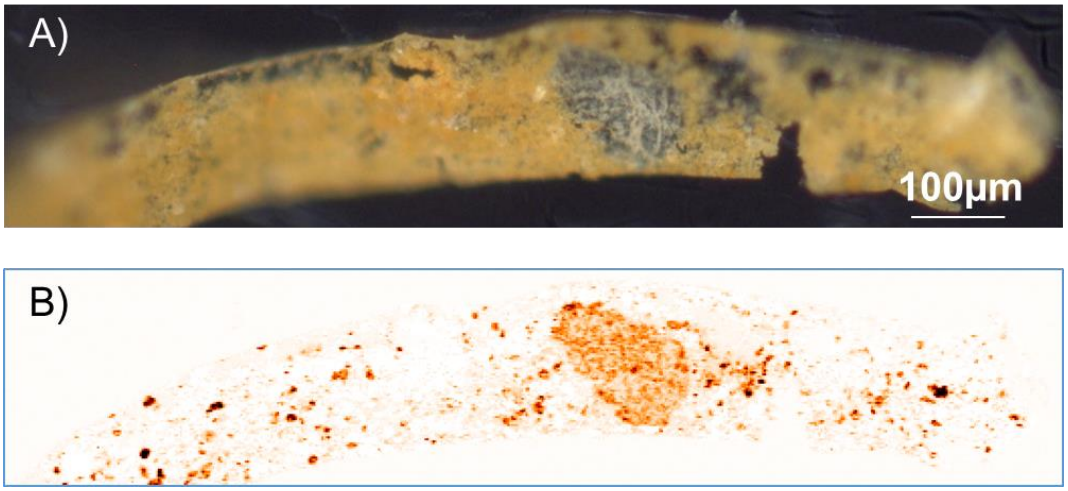

Figure S.2 : PN µXRD map in a 9-year old paint prepared following De Mayerne’s “huile de litharge” recipe.

Fig. S.3 shows the diffractogram collected on a simpler reconstruction of PbO grains dispersed in an cured-linseed oil droplet. Preparation was the following: fresh linseed oil was heated for 3h at T=110°C, and then simply spread on a glass slide. PbO particles were dispersed in this non-dried layer. The system has been aged for three months at 60°C in ambient atmosphere. µ-XRD measurements were performed at the I18 beamline of the DIAMOND light source (Didcot, UK), at E = 12.9 keV, with a beam of 2x2 µm². We observe that PN is now present, in combination with HC.

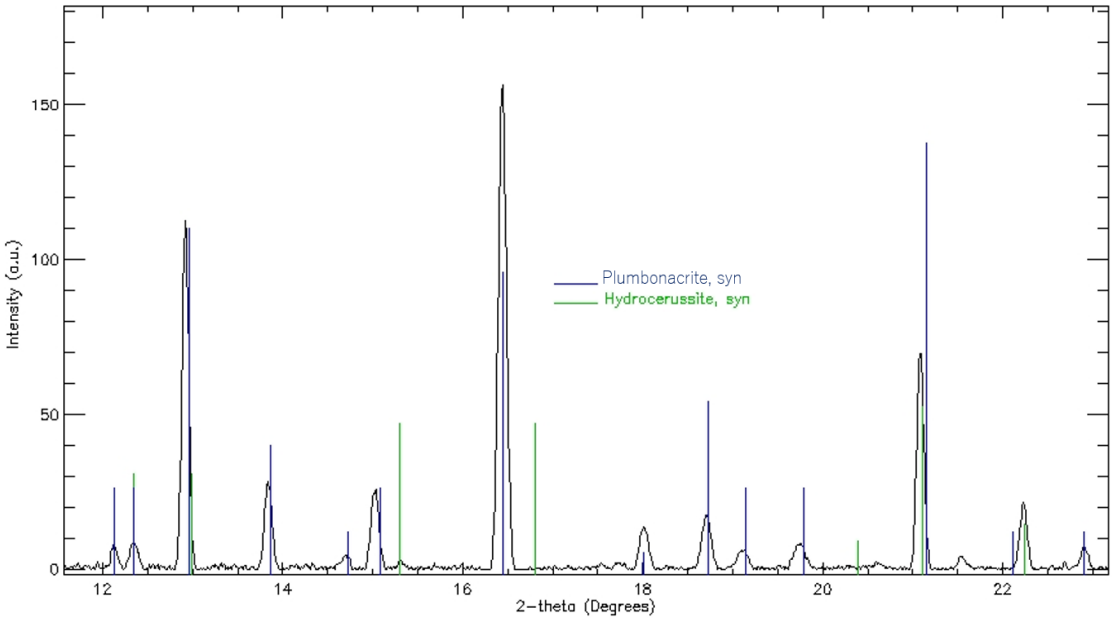

Figure S.3 : Diffractogram collected on a droplet of cured oil (heated without any Pb source) with dispersed PbO particles, left to dry for 3 months at 60°C.

References

[1] V. Gonzalez et al. (2016) Composition and microstructure of the lead white pigment in Masters paintings using HR Synchrotron XRD, Microchem. J., 2016, 125: 43-49

[2] V. Gonzalez et al. (2017) Synchrotron-based high angle resolution and high lateral resolution X-ray diffraction reveals lead white pigment qualities in Old Masters paintings, Anal. Chem 89(4): 13203-13211

[3] G. Ashiotis et al. (2015) The fast azimuthal integration Python library: pyFAI, J. App. Cryst., 48: 510-519

[4] W. De Nolf et al. (2014) XRDUA: crystalline phase distribution maps by two-dimensional scanning and tomographic (micro) X-ray powder diffraction, J. App. Cryst., 47: 1107-1117

[5] M. Cotte et al., Anal. Chem., 2016, 88, 6154–6160

[6] J. Rodriguez-Carvajal (1993) Recent advances in magnetic structure determination by neutron powder diffraction, Physica B, 192: 55-69.

[7] G. Chevrier et al. (1992), Neutron single-crystal refinement of cerussite, $PbCO_3$, and comparison with other aragonite-type carbonates, Zeit. Krist.199: 67-74.

[8] P. Martinetto, et al. (2002) Synthetic hydrocerussite, $2PbCO_3.Pb(OH)_2$, by X-ray powder diffraction, Acta Cryst. C, 58: 82-84.

[9] S.V. Krivovichev and P.C. Burns (2000) Crystal chemistry of basic lead carbonates. II. Crystal structure of synthetic 'plumbonacrite', Mineral. Mag. 64: 1069-1075.

[10] M. Cotte et al. (2017) ‘Lead soaps in paintings : Friends or foes?’, Studies in Conservation 62(1): 2-23

[11] M. Cotte et al. (2006) Kinetics of oil saponification by lead salts in ancient preparations of pharmaceutical lead plasters and painting lead mediums, Talanta 70(5): 1136-1142